doi:10.1111/evo.13396

Convergent selection pressures drive the evolution of rhodopsin kinetics at high altitudes via nonparallel mechanisms

Gianni M. Castiglione,[1,2] Ryan K. Schott,[2] Frances E. Hauser,[2] and Belinda S. W. Chang[1,2,3,4]

[1]*Department of Cell & Systems Biology, University of Toronto, Toronto, Ontario M5S 3G5, Canada*

[2]*Department of Ecology & Evolutionary Biology, University of Toronto, Toronto, Ontario M5S 3B2, Canada*

[3]*Centre for the Analysis of Genome Evolution and Function, University of Toronto, Toronto, Ontario M5S 3B2, Canada*

[4]*E-mail: belinda.chang@utoronto.ca*

Received August 9, 2017
Accepted November 2, 2017

Convergent evolution in response to similar selective pressures is a well-known phenomenon in evolutionary biology. Less well understood is how selection drives convergence in protein function, and the underlying mechanisms by which this can be achieved. Here, we investigate functional convergence in the visual system of two distantly related lineages of high-altitude adapted Andean and Himalayan catfishes. Statistical analyses revealed in the two high-altitude lineages, a parallel acceleration of evolutionary rates in rhodopsin, the dim-light visual pigment. However, the elevated rates were found to be accompanied by substitutions at different sites in the protein. Experiments substituting Andean- or Himalayan-specific residues significantly accelerated the kinetic rates of rhodopsin, destabilizing the ligand-bound forms. As found in cold-adapted enzymes, this phenotype likely compensates for a cold-induced decrease in kinetic rates, properties of rhodopsin mediating rod sensitivity and visual performance. Our study suggests that molecular convergence in protein function can be driven by parallel shifts in evolutionary rates but via nonparallel molecular mechanisms. Signatures of natural selection may therefore be a powerful guide for identifying complex instances of functional convergence across a wider range of protein systems.

KEY WORDS: **Codon models of molecular evolution, dim-light vision, G protein coupled receptor, high altitude catfish, molecular convergence, protein cold adaptation, visual pigment.**

Species that display convergent phenotypes have often experienced corresponding parallel changes in ecological selective pressures (Endler 1986; Losos 2011). Determining the molecular basis of convergently evolved phenotypes in response to changes in selection is a challenging new field of study (Stern 2013; Storz 2016). There are many compelling cases of phenotypic convergence mediated by parallel amino acid substitutions (Feldman et al. 2012; Projecto-Garcia et al. 2013; Storz 2016). However, phenotypic convergence is not always associated with amino acid parallelism; different substitutions targeting disparate molecular mechanisms can also produce convergent phenotypes (Rosenblum et al. 2010; Losos 2011; Natarajan et al. 2016). As such, nonparallel molecular convergence in proteins may be more widespread than previously appreciated (Tenaillon et al. 2012; Stern 2013; Storz 2016), particularly as identification of the underlying molecular mechanisms in such cases can be difficult (Rosenblum et al. 2010; Losos 2011; Natarajan et al. 2016). Furthermore, although amino acid parallelism is often used as a marker of functional convergence, it can be misleading when random background effects, rather than adaptive selection pressures, are involved (Parker et al. 2013; Foote et al. 2015; Thomas and Hahn 2015; Zou and Zhang 2015a,b). To address these issues, computational approaches that do not rely on amino acid parallelism, such as codon-based likelihood methods for selection analysis, can be employed to complement experimental investigations of amino acid variants.

Recent comparative studies suggest that estimating gene-specific evolutionary rates as convergent shifts in d_N/d_S relative to dissimilar outgroups can help identify candidate genes involved

in mediating molecular convergence in phenotypically convergent species (Chikina et al. 2016; Rubin and Moreau 2016; Partha et al. 2017). However, convergent molecular evolution can be driven by nonadaptive neutral forces and is considered common relative to the comparatively rare instances of adaptive convergence in molecular function (Foote et al. 2015; Zou and Zhang 2015a). Functional testing is therefore required to resolve whether convergence in molecular evolution reflects adaptive convergence in molecular function, which is ultimately required to link any finding of molecular convergence to the classical instances of organismal phenotypic convergence (Aminetzach et al. 2009; Brodie 2010). Environmentally induced shifts in the structural and functional constraints of proteins can be detected as corresponding changes in site-specific evolutionary rates (d_N/d_S) (Elde et al. 2009; Patel et al. 2012; Castiglione et al. 2017; Hauser et al. 2017), suggesting that similar ecological shifts may produce similar changes in site-specific d_N/d_S. Parallel shifts in evolutionary constraint may therefore, by extension, indicate similar shifts in function between orthologues exposed to common environmental pressures. To our knowledge, our approach of combining d_N/d_S computational analyses to detect convergently evolved rates with experimental investigations of protein function is novel, and may demonstrate great utility in revealing candidate mechanisms driving unpredictable instances of adaptive nonparallel convergence in protein function (Losos 2011; Natarajan et al. 2016).

Mountainous environments are a useful system in which to investigate molecular convergence, because ecological changes in pressure, temperature, and oxygen are predictably associated with altitude (Körner 2007; Natarajan et al. 2016). The Andes and Himalayas are two geographically distant and relatively young high-altitude environments (Gregory-Wodzicki 2000; Royden et al. 2008) where mountainous uplift has spurred rapid speciation and adaptation (Hughes and Eastwood 2006; Xing and Ree 2017). For example, high-altitude conditions have produced convergent adaptations to hypoxia that are known to be driven by nonparallel molecular convergence in Tibetan and Andean humans (Beall 2007) as well as birds (Jessen et al. 1991). Cold temperatures at high altitudes present additional challenges for ectotherms (Verberk et al. 2011), which inhabit drainages in both regions that can extend uninterrupted for thousands of vertical meters (Lujan and Conway 2015). Hydrologic forces imposed by rapid waters in these areas are extreme, offering ecological opportunities for organisms that can adapt to the physical challenges (Lujan and Conway 2015). However, little is known about how these high-altitude constraints may drive molecular convergence in aquatic species.

High-altitude catfish specialists, glyptosternoids and *Astroblepus*, occupy the Himalayan and the Andes mountains, respectively, and are distantly related, having diverged approximately 118 million years ago (Hedges et al. 2015). Both the Andean and Himalayan groups speciated during mountainous uplift (Schaefer 2011; Zhou et al. 2016), and display a striking morphological convergence that has evolved in response to rapidly flowing high-gradient headwaters (Guo et al. 2005; Peng et al. 2006; Lujan and Conway 2015). Unlike the closely related altitude generalists of each region (Guo et al. 2005; Peng et al. 2006; Schaefer et al. 2011), both Andean and Himalayan specialists are restricted to high altitudes, likely due to temperature-related physiological constraints (Schaefer et al. 2011; Ma et al. 2016). Although little is known of the molecular adaptations these fishes may have evolved in response to the decreased temperatures, the morphological and biogeographical similarities strongly suggest that these lineages have been subject to very similar high altitude related selection pressures.

The visual pigment rhodopsin (RH1) mediates dim-light vision in vertebrates, and has become a model for understanding molecular adaptation and functional convergence through amino acid parallelism (Hunt et al. 2001; Yokoyama et al. 2008). Natural variation in rhodopsin and the cone opsins is often associated with spectral tuning to the photic environment in the form of shifts in the pigments' wavelength of maximal absorbance (λ_{MAX}) (Hunt et al. 2001; Yokoyama et al. 2008; Cortesi et al. 2015; Dungan et al. 2016). These spectral shifts are largely mediated by amino acid substitutions at a limited number of sites within a few Angstroms of the retinal chromophore (~15–20) proximal enough to directly alter its electronic environment (Kochendoerfer et al. 1999). Rhodopsin detects photons through isomerization of its chromophore causing conformational changes that result in a series of equilibria among active-state rhodopsin intermediates, of which the metarhodopsin II (MII) form is thought to activate the second messenger G protein transducin, ultimately resulting in a neural signal (Ebrey and Koutalos 2001). Recently, it was demonstrated that the conformational stability of rhodopsin directly governs the kinetic rates of these rod equilibria (Schafer et al. 2016; Van Eps et al. 2017), which are temperature-sensitive and set a physiological limit on visual performance, as demonstrated in vivo (Aho et al. 1988; Kefalov et al. 2003; Imai et al. 2007; Frederiksen et al. 2016; Yue et al. 2017). The temperature dependence and physiological importance of these rod equilibria suggests that natural selection may alter rhodopsin stability as a means to modulate visual performance in response to natural temperature variation. Until recently, however, few studies have experimentally investigated how natural selection may drive visual adaptations through modulating the conformational stability of rhodopsin within different environments (Sugawara et al. 2010; Castiglione et al. 2017; Dungan and Chang 2017; Hauser et al. 2017). Although some rhodopsin mutations affecting these kinetic rates can also produce pleiotropic effects altering the spectral absorbance (λ_{MAX}) of rhodopsin (Gozem et al. 2012; Luk et al. 2016; Yue et al. 2017), there are other mutations affecting

stability that produce little to no effect on λ_{MAX} (Castiglione et al. 2017; Dungan and Chang 2017, Hauser et al. 2017), suggesting that in some environments it is protein stability, rather than spectral absorbance, that is specifically targeted by selection.

In a previous study, we found that the *rh1* of the Andean high-altitude specialist catfish genus, *Astroblepus* (Schaefer et al. 2011), was under positive selection relative to lowland catfishes at sites near key structural motifs known to control kinetic rates (Castiglione et al. 2017). Rare natural variants substituted into these sites accelerated both thermal- and light-activated decay rates of rhodopsin in vitro, likely by disrupting two distinct hubs of the intramolecular hydrogen-bond network that stabilizes dark-state and light-activated rhodopsin (Castiglione et al. 2017). This effect was consistent with cold adaptation in enzyme proteins that display adaptive mutations decreasing stability to improve activity relative to thermostable homologs at low temperatures (Siddiqui and Cavicchioli 2006; Fields et al. 2015; Åqvist 2017), and provided evidence that the functional constraints surrounding rhodopsin may vary with environmental temperature. Although our previous study was restricted to the Andean mountain range, here we investigate whether these temperature-related shifts in evolutionary constraints and kinetic rates may also be influencing rhodopsin in Himalayan catfish (Sisoridae), potentially targeting the same structural motifs. We tested this hypothesis using both computational and experimental approaches. Our computational results support a convergent shift in evolutionary constraint in RH1 occurring at *different* sites in Himalayan and Andean catfish rhodopsins. In the Himalayan catfish, this shift involved the introduction of rare amino acid variants into the *same* region of rhodopsin as one of the Andean catfish substitutions. In experimental mutagenesis studies of these high-altitude variants, we found that both Andean and Tibetan variants significantly accelerate the kinetic rates of dark- and active-state conformational decay, indicating convergent evolution of rhodopsin cold adaptation at high altitudes via differing molecular mechanisms.

Methods

DATASET ASSEMBLY

Rhodopsin-coding sequences (*rh1*) from Himalayan catfishes (Siluriformes: Sisoridae) were retrieved from GenBank and originate from a previous study (Zhou et al. 2016) (Table S1). *Rh1* sequences were also obtained from Characiform outgroups (Table S2), as well as from only those catfish lineages inhabiting lowland tropical and subtropical waters (see Table S3), which served as the lowland clade in our phylogenetic analyses. *Rh1* sequences originating from Andean catfishes (Siluriformes: *Astroblepus* and *Ancistrus*) were the same as those collected and processed in our previous study (Castiglione et al. 2017) and are publicly available (see Table S4). *Rh1* alignments were generated using PRANK codon alignment (Löytynoja and Goldman 2008) followed by manual verification. The final *rh1* alignment encoded for rhodopsin amino acid residues 42–307 (bovine RH1 numbering) inclusively. This encompassed the entire 7-transmembrane domain of rhodopsin.

PHYLOGENETIC AND MOLECULAR EVOLUTIONARY ANALYSES

To accurately evaluate selection pressures acting on Himalayan (Sisoridae) RH1 without the influence of background sequences on parameter estimates (Schott et al. 2014; Castiglione et al. 2017; Hauser et al. 2017), we used these alignments to construct two *rh1* datasets for phylogenetic analysis: (1) Himalayan (Sisoridae) catfishes, plus lowland outgroups ($n = 14$; see Fig. S1; referred to as the Himalayan-Lowland dataset); and (2) Himalayan (Sisoridae), Andean (*Astroblepus*, *Ancistrus*), and tropical siluriforms with characiform species as outgroups ($n = 78$; see Fig. S2; referred to as the Himalayan-Andean-Lowland dataset). For the Himalayan-Lowland dataset, a species tree was constructed by reference to established relationships and confidence estimates (Fig. S2) (Sullivan et al. 2006; Zhou et al. 2016). The Andean catfish phylogenetic relationships were those constructed in our previous study using Bayesian and maximum-likelihood methods to derive a well-supported consensus topology (Castiglione et al. 2017). The Himalayan and Andean catfish phylogenies were merged along with the addition of other siluriforms, as well as characiforms, all according to phylogenetic relationships (Sullivan et al. 2006; Chen et al. 2013). This formed the Himalayan-Andean-Lowland phylogeny used in subsequent PAML analyses.

We used codon models of molecular evolution from the PAML 4.7 software package (Yang 2007) to identify evidence of parallel shifts in evolutionary rates between Andean and Himalayan catfish *rh1*. First, we estimated the strength and form of selection acting on *rh1* from high-altitude Himalayan catfishes using the random sites models (M1, M2, M3, M7, M8) implemented in the codeml program. This required pruning out the lowland catfish outgroups from the Himalayan-Lowland dataset. We next employed PAML Clade models (Bielawski and Yang 2004) to explicitly test for differences in selective constraint between different clades within the Himalayan-Lowland dataset, as well as the Himalayan-Andean-Lowland dataset, which contained the characiform outgroups. For all PAML models, multiple runs with different starting priors were carried out to check for the convergence of parameter estimates. Tests of positive selection were done using random sites models, whereas tests of divergence were done using Clade model C and D (CmC and CmD) (Bielawski and Yang 2004), with M2aREL as the null model (Weadick and Chang 2012). CmC/D analyses tested for divergent selection between foreground and background branches or clades within the siluriform rhodopsin datasets. The foreground partition is listed after the underscore for the clade models (e.g., CmC_*foreground*).

In any partitioning scheme, all nonforeground data are present in the background partition. Parallel shifts in selective constraint in high altitude catfish *rh1* was tested for by conducting explicit tests of divergence between high altitude Himalayan and Andean catfish *rh1* evolutionary rates. This was done by conducting a CmC analysis on an alternative partitioning scheme treating each high-altitude specialist clade separately, and comparing the likelihood fit of that alternative model against the nested null CmC model treating the high-altitude groups as a single partition, using an LRT. CmC estimated site-specific posterior probabilities for respective molecular evolutionary tests. We consulted the presence of overlap in the posterior probabilities produced by the Bayes empirical Bayes (BEB) analysis (Yang et al. 2005) within these different methods as a first step in determining candidate sites for mutagenesis and in vitro functional experiments.

All PAML hypothesis testing was done by nested null-alternative model pairs, where the alternative model was statistically evaluated for significance by likelihood ratio tests (LRTs) with the null model using a χ^2 distribution as previously described (Anisimova et al. 2001; Yang 2007; Weadick and Chang 2012; Schott et al. 2014). Model fits were assessed by Akaike information criterion, where all other differences were relative to the best fitting model (ΔAIC). Sites under selection in any significant CmC-M2aREL model pair as assessed by LRT were predicted by BEB analysis (Yang et al. 2005) with confidence indicated as posterior probability (Yang 2007).

RHODOPSIN MUTAGENESIS AND EXPRESSION

Mutagenesis, expression, and purification procedures using the complete coding sequence of bovine (*Bos taurus*) rhodopsin in the pJET1.2 cloning vector (ThermoFisher Scientfic, Waltham, Massachusetts), as described in a previous study were used here (Castiglione et al. 2017). Briefly, site-directed mutagenesis procedures were used to create mutants, which were then transferred to the pIRES-hrGFP II expression vector (Stratagene, La Jolla, California) for transient transfection of HEK293T cells (Lipofectamine 2000, Invitrogen). Cells were harvested, regenerated with 5 μM 11-*cis*-retinal generously provided by Dr. R. Crouch (Medical University of South Carolina), solubilized in 1% dodecylmaltoside, and immunoaffinity purified using the 1D4 monoclonal antibody.

ABSORBANCE AND FLUORESCENCE SPECTROSCOPY

Spectroscopic assays were performed as described in previous studies (Castiglione et al. 2017). Briefly, the UV-visible absorption spectra of purified rhodopsin samples were recorded in the dark at 25°C using a Cary 4000 double-beam absorbance spectrophotometer (Agilent, Santa Clara, CA). λ_{MAX} values were determined by fitting dark spectra to a standard template curve (Govardovskii et al. 2000). Rhodopsin samples were light-activated for 30 sec using a fiber optic lamp (Dolan-Jenner, Boxborough, MA). The thermal decay of rhodopsin was monitored as the decrease in absorbance at λ_{MAX} in the dark, with temperature maintained by a Peltier-based temperature controller (Agilent). Mineral oil was added to prevent sample evaporation. Retinal release following rhodopsin photoactivation was monitored using a Cary Eclipse fluorescence spectrophotometer equipped with a Xenon flash lamp (Agilent). Rhodopsin samples were bleached for 30 sec at 20°C with a fiber optic lamp and fluorescence measurements were recorded at 30-sec intervals, using an excitation wavelength of 295 nm (1.5 nm slit width) and an emission wavelength of 330 nm (10 nm slit width).

Spectroscopic absorbance data were converted to their natural logarithm and plotted against time, and half-life values were calculated based on the slope b ($t_{1/2} = \ln 2/b$). Linear regressions used to calculate half-life values resulted in r^2 values greater than 0.95. Fluorescence data were fitted using a three variable, first-order exponential equation ($y = y_0 + a(1 - e^{-bx})$), and half-life values were calculated using the rate constant b ($t_{1/2} = \ln 2/b$). All curve fitting resulted in r^2 values greater than 0.95. Biological replicates were used ($n = 3$) to calculate dark-state λ_{MAX} values and retinal release half-lives, which were statistically assessed using a two-tailed *t*-test with unequal variance.

Results

ACCELERATED EVOLUTION IN HIMALAYAN CATFISH *Rh1*

We previously found evidence of divergent selection in Andean high-altitude specialist (*Astroblepus*) rhodopsin coding sequences (*rh1*) relative to that of lowland catfishes, with some sites displaying accelerated evolutionary rates (Castiglione et al. 2017). We hypothesized that high-altitude environments may have also placed unique selective constraints on Himalayan catfish (sisorids) *rh1*, specifically on the high-altitude specialist subfamily (glyptosternoids). To test this hypothesis, we used the codon-based likelihood models of molecular evolution implemented in PAML (Yang 2007) to characterize the selective pressures acting on Himalayan catfish *rh1* (see Methods). Rhodopsin coding sequences were obtained from GenBank, representing 12/13 extant sisorid genera, along with two closely related siluriform outgroups (see Table S1). The resulting alignment, along with the established multigene sisorid species tree (Zhou et al. 2016), were used in PAML analyses (see Fig. S1; Methods). To better understand the selection pressures acting on Himalayan *rh1*, we analyzed it as a distinct dataset using random sites models (Yang 2007). We found purifying selection acting on 90% of *rh1* codons (M3 (K = 2) $\omega_1 = 0.02$; Table 1), however, the other 10% of Himalayan catfish *rh1* codons displayed elevated evolutionary rates (M3 (K = 2) $\omega_1 = 0.93$; Table 1). A comparison of three-site (K = 3) versus

Table 1. Analyses of selection on Sisoridae rhodopsin (*rh1*) using PAML random sites models.

			Parameters[1]				
Dataset	Model	*ln*L	ω_0/p	ω_1/q	ω_2/ω_p	Null	P [df][2]
Sisoridae	M0	−2094.38	0.10	–	–	N/A	–
	M1a	−2066.50	0.02 (91%)	1.00 (9%)	–	M0	**0.000** [1]
	M2a	−2066.50	0.02 (91%)	1.00 (9%)	10.0 (0%)	M1a	1 [2]
	M3 (K = 2)	−2066.47	0.02 (90%)	0.93 (10%)	–	M0	**0.000** [2]
						M1	0.806 [1]
	M3 (K = 3)	−2066.47	0.00 (0%)	0.02 (90%)	0.93 (10%)	M0	**0.000** [4]
						M3 (K = 2)	1 [2]
	M7	−2066.69	0.04	0.374	–	N/A	–
	M8	−2066.69	0.04	0.375	1.00	M7	1 [2]

[1]ω values of each site class are shown for model M0–M3 (ω_0 – ω_2) with the proportion of each site class in parentheses. The M3 model was run with either two or three site classes (K). For M7 and M8, the shape parameters, *p* and *q*, which describe the beta distribution are listed instead. In addition, the ω value for the positively selected site class (ω_p, with the proportion of sites in parentheses) is shown for M8.
[2]Significant *P* values ($\alpha \leq 0.05$) are bolded. Degrees of freedom are given in square brackets after the *P* values.
ln L = ln likelihood; *P* = *P*-value; N/A = not applicable.

two-site class (K = 2) M3 models suggested that two site classes were sufficient for modeling evolutionary rate variation among Himalayan catfish *rh1* sites ($P = 1$; Table 1). Unlike our previous analyses on the Andean catfish *rh1*, we found no evidence for positive selection in Himalayan catfish *rh1* (Table 1). The small size of the Himalayan catfish *rh1* dataset may have reduced the power of our analyses to detect positive selection (Yang 2007).

We combined the Himalayan *rh1* dataset with closely related lowland catfish *rh1*, and next investigated evidence for accelerated evolutionary rates in Himalayan (*Sisoridae*) catfish relative to the lowland lineages ("Tropical lowland" clades represented in Fig. S2). We tested this hypothesis explicitly by using PAML CmC and CmD (Bielawski and Yang 2004), which test for a divergently selected class of sites in two or more clades. Separating all Himalayan catfish *rh1* from that of lowland catfish outgroups resulted in significant evidence for accelerated evolutionary rates in the Himalayan clade (CmD_*Sisoridae clade*, divergent site class ω (ω_d) = 0.96 vs. 0.28 in lowland outgroups, $P = 0.037$; Table 2). A BEB analysis identified a subset of sites with posterior probabilities of belonging to the divergent site class. Consistent with our hypothesis, we also found that evolutionary rates were most strongly accelerated in a nested high-altitude specialist clade, which was significantly divergent even from the basal sisorids (CmD_*Glypto clade*, $P < 0.001$; Table 2). Evolutionary constraints on a subset of *rh1* sites from these high-altitude specialists appeared to be significantly relaxed relative to all other background catfish taxa ($\omega_d = 1.69$ vs. 0.48, respectively; Table 2), and were different from those identified in the rest of the Himalayan clade. There was also evidence for divergence (CmC_*Glypto branch* vs. M2a_rel $P = 0.03$; Table 2) and positive selection (CmC_*Glypto branch* vs. CmC_*fix* $P = 0.03$; Table 2) along the branch leading to the high-altitude specialist clade, but not along the branch leading to the entire Himalayan clade (CmC_*Sisoridae branch* $P = 0.437$; Table 2). These results suggest that a period of accelerated *rh1* evolutionary rates and positive selection accompanied the diversification of the high-altitude specialist subfamily specifically.

PARALLEL SHIFT IN SELECTIVE CONSTRAINT ON HIMALAYAN AND ANDEAN HIGH-ALTITUDE SPECIALIST *Rh1*

Because we found unique selection pressures accelerating evolutionary rates in both Himalayan and Andean (Castiglione et al. 2017) high-altitude specialist *rh1*, we next tested whether, relative to lowland catfishes, similar shifts in evolutionary constraints on *rh1* existed between the two high-altitude groups. We constructed a large catfish *rh1* dataset for phylogenetic analysis (see Fig. S2), which contained both Andean (*Astroblepus* and *Ancistrus*) and Himalayan (sisorids and nested subfamily glyptosterninae) clades, as well as subtropical/tropical lowland catfishes and characiform outgroups (Figs. 1A and S2). We conducted CmC analyses on various partitions of this dataset to test the hypothesis that *rh1* from high-altitude specialist clades underwent parallel shifts in evolutionary rates distinct from that of other catfishes. This was done by first testing multiple nested evolutionary models (Schott et al. 2014; Dungan et al. 2016; Castiglione et al. 2017; Hauser et al. 2017). We detected significant evidence of accelerated evolutionary rates in Andean high-altitude specialist *rh1* (Fig. 1B, Andean; Table 3; CmC_*Astro*, $P = 0.03$), reproducing our earlier result within the current expanded dataset (Castiglione et al. 2017). We also detected significant evidence of accelerated evolutionary rates in Himalayan high-altitude specialist *rh1* (Fig. 1C, Himalayan; Table 3; CmC_*Glypto*, $P = 0.004$). These

Table 2. Results of Clade model C (CmC) and D (CmD) analyses of *rh1* on the Sisoridae species tree with outgroups under various partitions.

Model and foreground[1]	ΔAIC[2]	ln*L*	Parameters[3] ω_0/p	ω_1/q	ω_2/ω_d	Null	*P* [df][4]
M3 (k = 2)	9.14	−2302.61	0.02 (91%)	0.83 (9%)	–	–	–
M3 (k = 3)	13.1	−2302.61	0.02 (24%)	0.02 (66%)	0.83 (9%)	M3 (K = 2)	1 [2]
M2a_rel	11.7	−2302.91	0.02 (91%)	1 (0%)	0.83 (9%)	N/A	–
CmC_*Sisoridae clade*	8.80	−2300.44	0.02 (91%)	1 (0%)	0.28 (9%) Sis:0.96	M2a_rel	**0.026** [1]
CmC_*Glypto clade*	1.46	−2296.77	0.02 (91%)	1 (2%)	0.32 (7%) Gly:1.98	M2a_rel	**0.000** [1]
						CmC_fix	0.114 [1]
CmC_*Glypto clade w fix*	1.96	−2298.02	0.01 (89%)	1 (4%)	0.17 (7%) Gly: 1.00	N/A	–
CmC_*Sisoridae branch*	13.1	−2302.61	0.01 (89%)	1 (6%)	0.49 (5%) Sis: 0.00	M2a_rel	0.437 [1]
CmC_*Glypto branch*	9.01	−2300.55	0.02 (91%)	1 (4%)	0.59 (5%) Gly: 4.48	M2a_rel	**0.030** [1]
						CmC_fix	**0.030** [1]
CmC_*Glypto branch w fix*	11.7	−2302.91	0.02 (91%)	1 (8%)	4.80 (0%) Gly: 1.00	N/A	**–**
CmD_ *Sisoridae clade*	6.80	−2300.44	0.02 (91%)	–	0.28 (9%) Sis: 0.96	M3 (K = 2)	**0.037** [1]
CmD_*Glypto clade*	**0***	−2297.04	0.02 (91%)	–	0.48 (9%) Glyp: 1.69	M3 (K = 2)	**0.001** [1]
						CmC_fix	0.112 [1]
CmD_*Glypto clade w fixed*	0.53	−2298.31	0.01 (89%)	–	0.42 (11%) Glyp: 1.00	N/A	–
CmD_*Sisoridae branch*	10.9	−2302.51	0.02 (91%)	–	0.82 (9%) Sis: 2.03	M3 (K = 2)	0.642 [1]
CmD_*Glypto branch*	7.34	−2300.71	0.02 (91%)	–	0.78 (9%) Glyp: 3.17	M3 (K = 2)	0.051 [1]

[1]The foreground partition is listed after the underscore for the clade models and consists of either Sisoridae or Glyptosternoids (*Glypto*) clades or branches leading to the clade. In certain CmC models ω is fixed to 1 (*w fix*; CmC_fix). In any partitioning scheme, all nonforeground data are present in the background partition. M3 models were run with either two or three site classes (K).

[2]The model with a ΔAIC (Akaike information criterion) value of 0 is the best fit. All other ΔAIC values are calculated from the AIC of that model. The best fit is bolded with an asterisk (*).

[3]ω_d is the divergent site class, which has a separate value for the foreground and background partitions.

[4]Significant *P* values ($\alpha \leq 0.05$) are bolded. Degrees of freedom are given in square brackets after the *P* values.

ln L = ln likelihood; *P* = *P* value; AIC = Akaike information criterion.

results suggest that *rh1* from both Himalayan and Andean high-altitude catfish specialists have undergone a highly similar shift in evolutionary constraint relative to the lowland catfishes, as well as to the closely related generalists in both geographic regions.

Due to this similarity, we next tested whether the accelerated evolutionary rates within the *rh1* of the high-altitude specialists (Fig. 1A) could be better described with a single evolutionary rate parameter (ω_d), which would be evidence for a comparable convergent shift in both high-altitude groups relative to the lowland taxa. We used a CmC model containing the high-altitude specialists from the Andes (*Astroblepus*) and the Himalayas (glyptosternoids) as a single partition (Fig. 1B, high altitude one-partition), compared against all other catfish *rh1*. This model yielded highly significant evidence for parallel shifts in the evolutionary rates between *Astroblepus* and Glyptosternoid *rh1* (Fig. 1B, high altitude one-partition; Table 3; CmC_*High Alt Convergent*, $P < 0.001$), outperforming the previously tested models (in which each high-altitude group was treated as a separate partition; Fig. 1B, Andean, Himalayan, ΔAIC values). We next tested the alternative hypothesis that Andean and Himalayan groups displayed selective pressures distinct from each other by using a high altitude two-partition model estimating a separate ω_d for *Astroblepus*, glyptosternoids, and other catfishes (Fig. 1B, high altitude two-partition). A likelihood-ratio test (LRT) with the one-partition high altitude model as the nested null hypothesis rejected this alternative model (CmC_*Astro* vs. *Glypto*, $P = 1$; Table 3), providing evidence for the sufficiency of a single evolutionary rate parameter to describe the similar shifts in the selective constraints acting on each high-altitude *rh1* relative to lowland catfishes. To investigate the robustness of these results to changes in underlying tree topology, we created four alternative species phylogenies by permuting key relationships within the different catfish clades (Fig. S2). PAML analyses (CmC) treating high-altitude specialists from the Andes (*Astroblepus*) and the Himalayas (glyptosternoids) as a single partition using these permuted phylogenies still produced highly significant evidence for parallel shifts in the evolutionary rates between *Astroblepus* and Glyptosternoid *rh1*, with nearly identical parameter estimates to those generated from analyses using the undistorted species phylogeny (Table S5; $P < 0.003$). Altogether, these results strongly

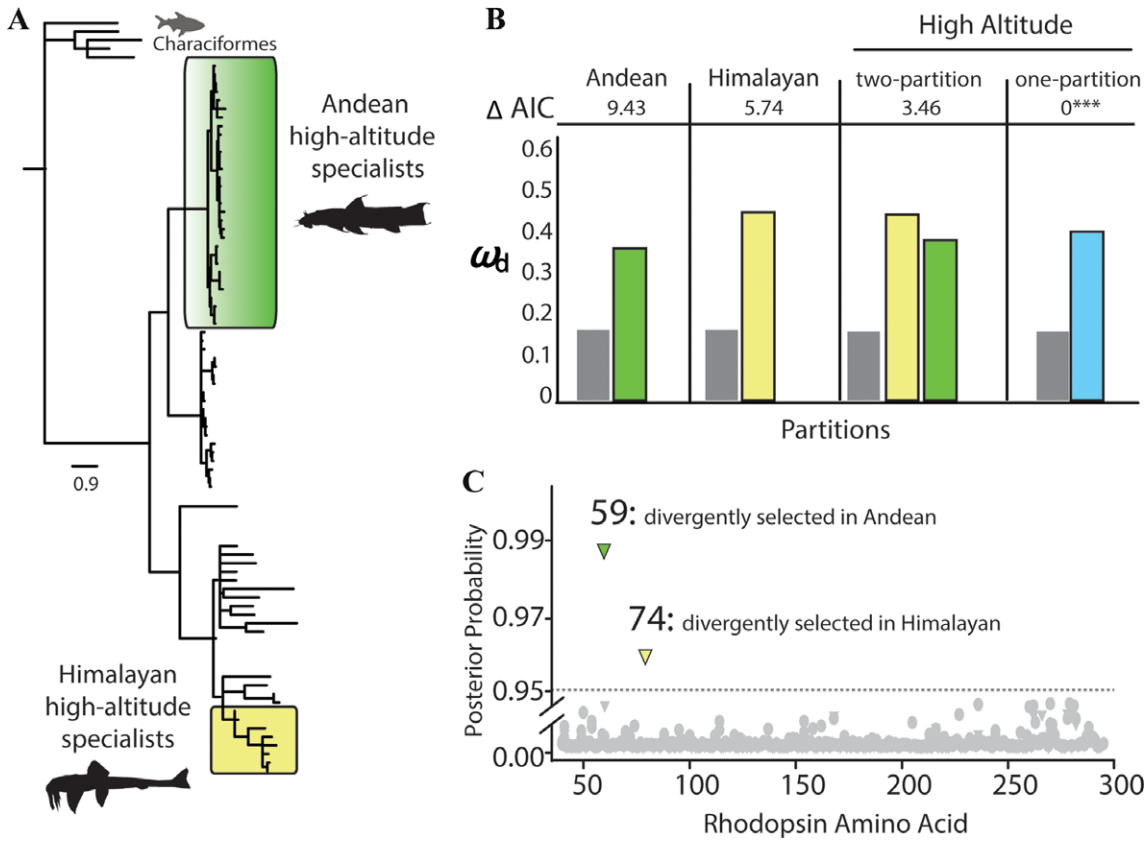

Figure 1. Parallel evolutionary rates in Andean and Himalayan high-altitude catfish *rh1*. *Rh1* from Andean (*Astroblepus*; green) and Himalayan (*Glyptosterninae*; yellow) high-altitude specialists are under parallel shifts in evolutionary constraint. (A) Clade model C (CmC) analyses of high-altitude *rh1* were conducted on a siluriform species tree containing characiform outgroups. Scale bar represents number of nucleotide substitutions per codon. (B) Significant CmC models were assessed by likelihood-ratio tests with null model M2aREL, with reference to a χ^2 distribution as previously described (Yang 2007; Weadick and Chang 2012; Schott et al. 2014). This provided evidence ($P < 0.05$; see Table 3) for divergent molecular evolutionary rates (ω_d) between *rh1* from foreground (green, *Astroblepus*; yellow, glyptosternoids) and background (gray) partitions. The high-altitude one-partition model (blue) consists of *Astroblepus* and glyptosternoids as a single partition, and all others in the background. Model fits were assessed by Akaike information criterion differences to the best fitting model (ΔAIC). (C) Rhodopsin sites mediating the parallel acceleration of evolutionary rates in the high-altitude specialists were predicted by Bayes empirical Bayes (BEB) analysis (Yang et al. 2005) with confidence indicated as posterior probability (Yang 2007). Comparison of BEB sites across all CmC analyses revealed that sites 59 and 74 are divergently selected exclusively within each high-altitude region, respectively, which suggests a parallel acceleration of evolutionary rates targeting different structural mechanisms.

suggest that despite vast geographic and phylogenetic separation, high-altitude specialists from the Andes and the Himalayas possess an *rh1* with codon sites evolving under accelerated evolutionary rates. These high-altitude rates are together divergent relative to any other catfish lineage, including the sister clades of altitude generalists in each respective region (Fig. 1B, Table 3).

CONVERGENT SELECTION PRESSURES IN HIGH-ALTITUDE ANDEAN AND HIMALAYAN *RH1* TARGET DIFFERENT SITES

Rh1 from Himalayan and Andean high-altitude catfish specialists has undergone a convergent shift in evolutionary constraint relative to warm-water dwelling lowland catfishes, as well as to closely related high-altitude generalists in each region. Interestingly, when the two high-altitude specialist groups are combined into a single partition (Fig. 1B, high altitude one-partition), a single set of rhodopsin sites are identified under the divergent site class (Fig. 1C, Table S6). After applying a posterior probability cut-off of >0.95 to the CmC BEB analysis (BEB; Table S6; Methods), two sites were implicated as mediating these parallel shifts in selective constraint: sites 59 and 74 (Fig. 1C; Table S6). Interestingly, sites 59 and 288 were previously identified to mediate rhodopsin cold adaptation in the Andean catfishes (Castiglione et al. 2017). When the Andean and Himalayan clades are analyzed separately (Fig. 1B, Andean, Himalayan), the BEB analysis identifies nonoverlapping sites between the rhodopsins from the two

Table 3. Results of Clade Model C (CmC) analyses of *rh1* on the siluriform species tree under various partitions.

Model and foreground[1]	ΔAIC[2]	ln*L*	Parameters[3] ω_0/p	ω_1/q	ω_2/ω_d	Null	*P* [df][4]
M2a_rel	11.8	−6002.57	0.17 (22%)	1 (7%)	0.00 (71%)	N/A	-
CmC_*Astro*	9.43	−6000.36	0.00 (73%)	1 (6%)	0.17 (21%) Astro: 0.37	M2a_rel	**0.03** [1]
CmC_*Glypto*	5.74	−5998.52	0.00 (73%)	1 (6%)	0.17 (21%) Gly: 0.43	M2a_rel	**0.004** [1]
CmC_*High Alt Convergent*	**0***	−5995.65	0.00 (74%)	1 (6%)	0.15 (20%) High Alt: 0.41	M2a_rel	**0.000** [1]
CmC_*Astro vs. Glypto*	**3.46***	−5996.37	0.00 (74%)	1 (6%)	0.15 (20%) Ast: 0.39 Gly:0.45	M2a_rel	**0.002** [2]
						CmC_High Alt Conver	1 **[1]**
CmC_*Sisoridae*	54.0	−6022.65	0.00 (71%)	1 (7%)	0.17 (22%) Sis: 0.19	M2a_rel	1 [1]
CmC_*Highlands*	50.5	−6020.94	0.00 (73%)	1 (6%)	0.15 (21%) High: 0.26	M2a_rel	1 [1]
CmC_*Sisoridae/Astro*	50.34	−6019.82	0.00 (73%)	1 (6%)	0.15 (21%) Ast: 0.38 Sis: 0.20	M2a_rel	1 [2]
CmC_*Siluri/Characi*	52.02	−6021.65	0.00 (72%)	1 (6%)	0.14 (22%) Sil:0.18	M2a_rel	1 [1]

[1]The foreground partition is listed after the underscore for the clade models and consists of either: siluriforms and characiform clades separately (*Siluri/Characi*; *Sil*); the highland catfish group Sisoridae (*Sis*); the two high altitude specialist groups *Astroblepus* (*Astro*; *Ast)* and Glyptosternoids (*Glypto*; *Gly*); Sisoridae and *Astroblepus* together (*Highlands*; *high*), separately (*Sisoridae/Astro*), or *Astroblepus* and Glyptosternoids together (*high alt convergent; high alt; high alt*) or separately (*Astro* vs. *Glypto*). In any partitioning scheme, the entire clade was tested, and all nonforeground data are present in the background partition.

[2]All ΔAIC values are calculated from the lowest AIC model. The top two best fits are bolded with an asterisk (*).

[3]ω_d is the divergent site class, which has a separate value for the foreground and background partitions.

[4]Significant *P* values ($\alpha \leq 0.05$) are bolded. Degrees of freedom are given in square brackets after the *P* values.

ln L = ln likelihood; *P* = *P*-value, AIC = Akaike information criterion.

high-altitude regions (Table S6). This suggests that the functional constraints imposed on rhodopsin by these geographically distant high-altitude environments are similar, but target different sites in the Andean (site 59) and Himalayan (site 74) catfish rhodopsins.

This hypothesis is supported by an analysis of RH1 amino acid variation across vertebrate rhodopsins. Site 59 displays a rare natural variant (Q59) in the Andean specialist *rh1* that is completely conserved as L59 in all vertebrates including the Himalayan specialist (Fig. 2A and B). Conversely, site 74 displays a rare natural variant (F74) in the Himalayan specialist *rh1* that is strongly conserved as Y74 in all vertebrates including the Andean specialist (Fig. 2A and B). In each of Andean and Himalayan high-altitude specialist *rh1*, there are four instances of Q59 and F74 in each respective lineage (Fig. S3), both of which are encoded by a nonsynonymous single nucleotide substitution consisting of an A/T nucleotide transversion event at the second-codon position (Table S7). This suggests that the functional constraints surrounding the rhodopsin of these two high-altitude specialist lineages has varied relative to lowland lineages in each geographic region (Bofkin and Goldman 2007). Strikingly, both sites 59 and 74 are only 8 Å apart within the dark-state rhodopsin crystal structure (Okada et al. 2004) (Fig. 2C) located on transmembrane helices (TM) 1 and 2, respectively (Fig. 2D and E). Consistent with the molecular mechanisms of cold adaption (Siddiqui and Cavicchioli 2006; Fields et al. 2015; Åqvist 2017), both sites are membrane facing, and are proximal to the same two highly conserved class A G protein coupled receptor (GPCR) motifs controlling conformational stability (Fig. 2D and E). The first of these motifs centers around Y306, which is part of the ultraconserved class A GPCR NPxxY motif of TM7 that modulates the MI–MII equilibrium (Hofmann et al. 2009). Located on TM1 and TM2 are important residues directly adjacent to sites 59 and 74 that either directly interact with Y306 (T58; Venkatakrishnan et al. 2016) or form indirect hydrogen bonds with it via a predicted water molecule (T62, N73) (Okada et al. 2004; Palczewski 2006). Sites 59 and 74 are also on the periphery of the complex TM1–TM2–TM7 network,

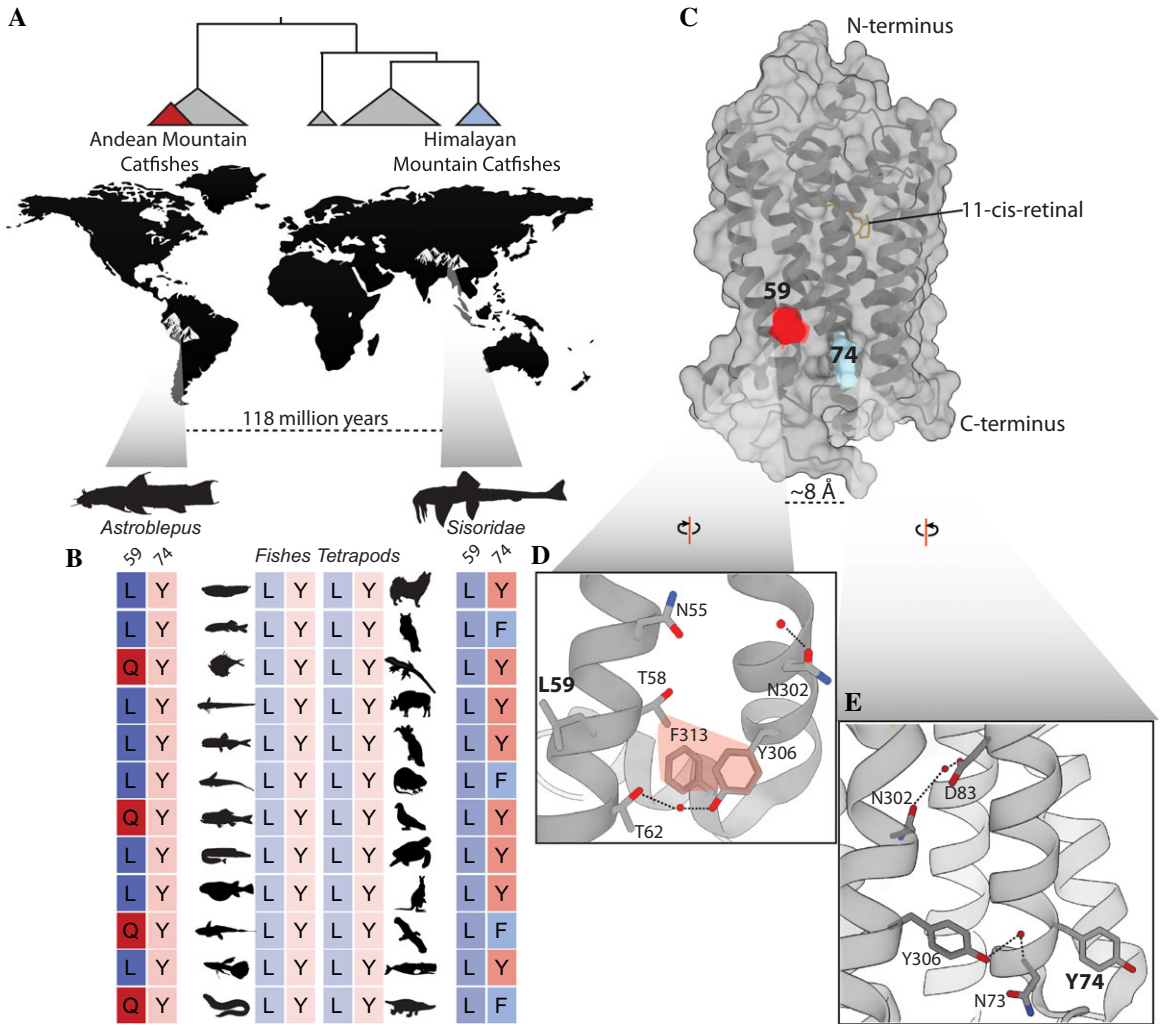

Figure 2. **Similar selection pressures in Andean and Himalayan *rh1* are targeted to distinct sites near the same structural motif. High-altitude specialist catfishes from the Andes (*Astroblepus*) and the Himalayas (*Sisoridae*) have *rh1* codon sites (59 and 74, respectively) that have undergone a parallel shift in evolutionary constraint. (A) High-altitude groups are separated by approximately 118 million years of evolutionary divergence (Hedges et al. 2015). (B) Each displays rare natural variation at a convergently evolving site (59, 74) not observed in any known vertebrate rhodopsin. Variation is mutually exclusive between each high-altitude group and occurs repeatedly across different lineages in the Andean and Himalayan clades (see Fig. S3 for details). (C) Convergently evolving sites 59 and 74 are both membrane-facing residues located only 8 Å apart in the rhodopsin dark-state crystal structure (PDB ID: 1U19; Okada et al. 2004). Each site is proximal to members of the same important structural motifs of rhodopsin (D, E), which can consist of direct interactions (red highlight) and/or hydrogen bonds (dashed lines) between residues and water molecules (oxygen atoms, red spheres).**

a stabilizing motif in both the rhodopsin dark state as well as the light-activated MII state (Hofmann et al. 2009; Ernst et al. 2014). This motif includes a hydrogen bond between N55 and D83, and an indirect H-bond link between D83 and N302 (another member of the NPxxY motif) via a water molecule (Okada et al. 2004; Hofmann et al. 2009; Ernst et al. 2014). Our structural analysis suggests that these highly conserved functional domains may be modulated by natural variation at sites 59 (L/Q) and 74 (Y/F), which would suggest that natural selection has targeted these sites due to their potential capacity to modulate rhodopsin kinetics at high altitudes.

ANDEAN- AND HIMALAYAN-SPECIFIC AMINO ACID VARIANTS MODULATE RHODOPSIN KINETICS

Given the distance of these mutations from the retinal binding pocket (RBP; Fig. 2C), which controls spectral tuning (Kochendoerfer et al. 1999), we hypothesized that the parallel shift of evolutionary constraint at sites 59 and 74 reflected nonspectral temperature-related shifts in rhodopsin functional constraints in response to cold high-altitude environments (Castiglione et al. 2017). We tested the functional relevance of these evolutionary and structural predictions using the model rhodopsin protein (*B. taurus*; bovine) (Schafer et al. 2016), which, as the

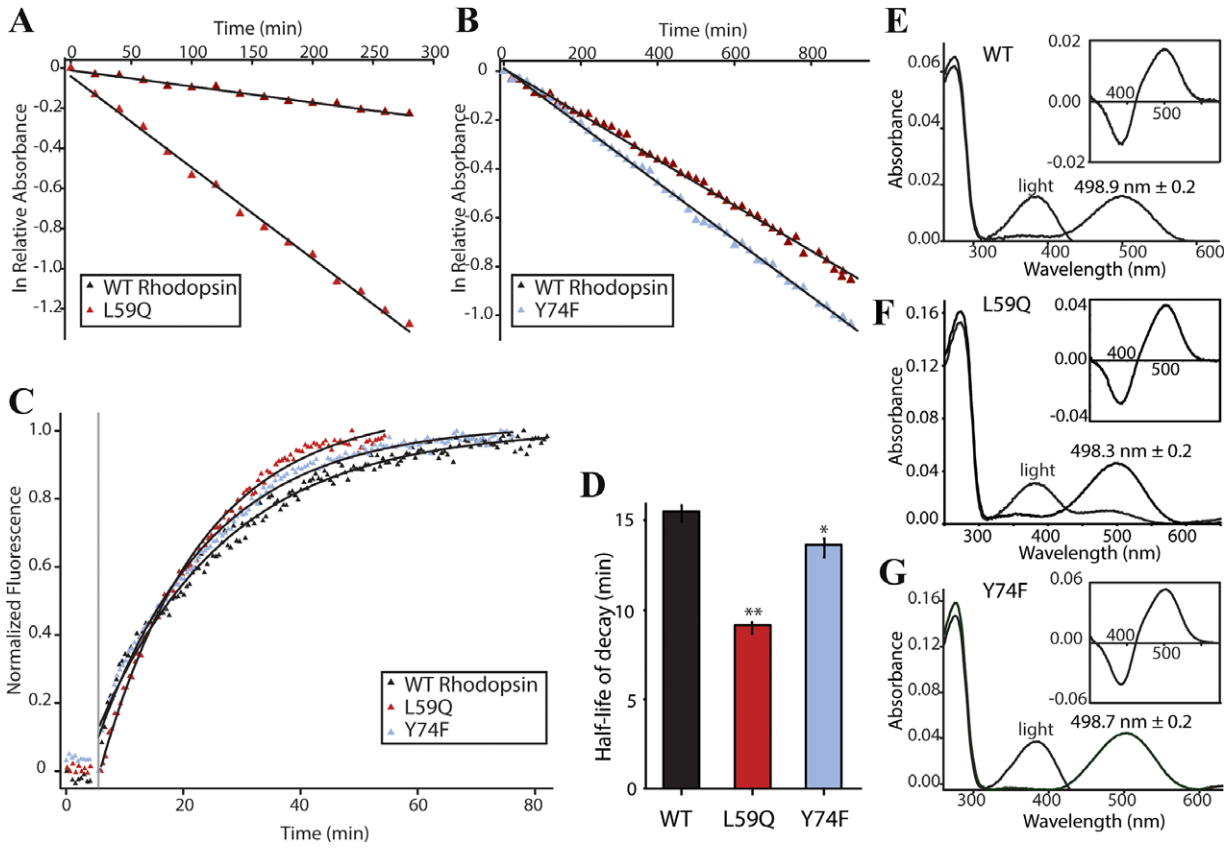

Figure 3. **Parallel shifts in evolutionary constraint target sites controlling the kinetic rates of dark- and light-activated rhodopsin. (A, B) Decay of dark-state WT and mutant rhodopsins at 45°C, assayed by monitoring decreasing absorbance at λ_{MAX} in the dark over time. Absorbance data converted to its natural logarithm and plotted against time with half-life values calculated from the rate constant and made relative to WT. (C) Decay of active-state (MII) WT, L59Q (Castiglione et al. 2017), and Y74F rhodopsins assayed by monitoring increasing fluorescence intensity upon release of all-*trans*-retinal after exposure to light (vertical line). Lines are data fits with first-order exponential equations, with half-life values calculated from the rate constant. (D) Differences in WT versus L59Q ($P < 0.001$) and WT versus Y74F ($P = 0.02$) rhodopsin retinal release half-life values were statistically assessed using a two-tailed *t*-test with unequal variance (see main text and Methods). SE is shown. UV-vis absorbance spectra of dark-state and light-activated (E) WT, (F) L59Q (Castiglione et al. 2017), and (G) Y74F with dark-state λ_{MAX} values shown. All insets show difference spectra, indicating photoactivation after exposure to light.**

prototypical class A GPCR, allows interpretation of results within well-resolved crystal structures (Okada et al. 2004; Ernst et al. 2014). We used site-directed mutagenesis to introduce L59Q and Y74F (found in Andean and Himalayan high-altitude specialists, respectively; Fig. 2A and B) into bovine rhodopsin (see Methods).

We had previously demonstrated that the L59Q substitution found in Andean high-altitude specialist *rh1* significantly destabilized rhodopsin, accelerating the decay of both active and inactive ligand-bound forms (Castiglione et al. 2017)—a functional phenotype consistent with cold-adaptation in enzymes (Fields et al. 2015). We therefore tested whether the unique Himalayan substitutions at site 74 (Y74F) also shifted rhodopsin kinetics in the same direction as the Andean substitution L59Q. We first measured the thermal decay of dark-state wild-type rhodopsin and the two mutant pigments to test if the mutations at each site accelerated the destabilization of rhodopsin toward spontaneous thermal activation (Guo et al. 2014). This was accomplished by monitoring the decrease of absorption at dark-state λ_{MAX} while incubating at 45°C, a process caused by a combination of thermal isomerization and/or spontaneous hydrolysis of the Schiff base linkage (Guo et al. 2014). Consistent with our previous results (Castiglione et al. 2017), we found that relative to wild-type rhodopsin, the L59Q substitution dramatically accelerated the half-life of thermal decay (rel-$t_{1/2} = 0.2$; Fig. 3A). Interestingly, the Y74F substitution also accelerated the half-life of thermal decay, but to a lesser degree (rel-$t_{1/2} = 0.75$; Fig. 3B, Table 4).

We next monitored all-*trans*-retinal release in rhodopsin following photoactivation at 20°C using a fluorescence assay (see Methods), which has been validated recently as a reliable method for tracking light-activated MII decay (Schafer et al. 2016). The half-life value of retinal release for wild-type rhodopsin was 15.5 ± 0.05 min (Fig. 3C and D), consistent with previously

Table 4. Summary of spectroscopic assays on wild-type and mutant rhodopsins.

	$\lambda_{MAX\ (nm)}$[1,2]	Half-life of retinal release[1,2]	Relative half-life of thermal decay
Wild-type bovine rhodopsin	498.9 ± 0.2 (3)	15.5 ± 0.05 (3)	1.00
L59Q	498.3 ± 0.2 (5)	9.2 ± 0.3 (4)[3]	0.20
Y74F	498.7 ± 0.2 (3)	13.6 ± 0.5 (3)	0.75

[1]SE is shown.
[2]Number of biological replicates is shown in parentheses.
[3]Values are from Castiglione et al. (2017).

published results (Schafer et al. 2016; Dungan and Chang 2017). Similar to our thermal decay experiments, we found that Y74F also accelerated rhodopsin retinal release, but to a lesser degree than the L59Q substitution (13.6 ± 0.5 min and 9.2 ± 0.3 [Castiglione et al. 2017], respectively; Fig. 3C and D, Table 4). Nevertheless, MII decay was significantly accelerated relative to wild-type by both L59Q (t = 14.6, degrees of freedom [df] = 6, P <0.001) and Y74F (t = 3.6, df = 4, P = 0.02) (Fig. 3 D; Table 4). These results suggest that natural variation at sites undergoing a parallel shift in evolutionary constraint may be promoting increased kinetic rates in the rhodopsin pigments of high-altitude specialists from the Andes and the Himalayas.

We next explored whether these sites could be experiencing a parallel acceleration of evolutionary rates in response to putative spectral shifts in high-altitude ambient light spectra. Purified wild-type rhodopsin produced a λ_{MAX} of 498.9 nm ± 0.2, similar to other published results (Fig. 3E; Table 4) (Dungan and Chang 2017). We had found previously that L59Q did not affect rhodopsin spectral tuning (Fig. 3F), which is consistent with constant spectral conditions within clear mountainous streams (Castiglione et al. 2017). Here, we find that Y74F rhodopsin also has very limited effects on spectral tuning, with an almost identical λ_{MAX} value to both wild-type and L59Q rhodopsin (Fig. 3E–G). When bleached with light for 30 sec, the λ_{MAX} values of wild-type, L59Q, and Y74F rhodopsin all shifted to ∼380 nm, characteristic of the biologically active MII intermediate (Schafer et al. 2016) (Fig. 3E–G), suggesting that the substitutions do not interfere with the pigment's normal light-detecting functions. These results strongly suggest that a parallel shift of selective constraint at high altitudes is not targeting sites 59 and 74 to alter rhodopsin spectral sensitivity, which is consistent with their location outside the RBP (Fig. 2B).

Discussion

Using both computational and experimental methods, we tested for convergence in evolutionary rate and function in high-altitude Andean (*Astroblepus*) and Himalayan catfish (glyptosterninae) rhodopsins. We found evidence that between these two environments, parallel selection pressures have targeted different rhodopsin sites located near the same two structural motifs stabilizing the ligand-bound rhodopsin structure. Substituting natural high-altitude amino acid variants at these sites found in Andean (L59Q) and Himalayan (Y74F) rhodopsin accelerated dark-state and light-activated decay rates relative to a control pigment. Here, we discuss our results in the context of high-altitude rhodopsin evolution, the ecology and evolutionary history of these two high-altitude catfish groups, and molecular convergence in proteins. We propose that the evolution of rhodopsin function at high altitudes illustrates why a previously underexplored relationship between evolutionary rate and functional convergence should be further disentangled and scrutinized.

ADAPTIVE FUNCTIONAL CONVERGENCE IN RHODOPSIN KINETICS AT HIGH ALTITUDES

High altitude environments impose a variety of biochemical and physiological challenges for organisms, such as hypoxia, low atmospheric pressure, and cold temperatures (Hayes et al. 1999; Beall 2007; Storz et al. 2007). Ecological divergence between high and low altitude environments may therefore drive rapid rates of diversification across high altitude organismal genomes, as suggested in both Andean (Hughes and Eastwood 2006; Nevado et al. 2016) and Himalayan systems (Xing and Ree 2017). This suggests that the parallel acceleration of evolutionary rates we detected here in high-altitude Andean and Himalayan catfish specialist *rh1* may be a consequence of a genome-wide acceleration of molecular evolutionary rates within these lineages. Nevertheless, the amino acid variants in RH1 detected at sites evolving under accelerated rates in our analyses produce consistent and measurable shifts in protein function. As we describe in detail below, the physiological relevance and temperature sensitivity of rhodopsin conformational stability, combined with the molecular mechanisms of cold-adaptation in proteins, likely explains why natural variants in distinct regions of rhodopsin are under accelerated evolutionary rates within these fishes.

Visual performance in organisms is reliant not only on wavelength detection, but also on the neural signaling of rod photoreceptors, which is initiated by rhodopsin-mediated phototransduction. This proceeds through a complex series of inactive- and active-state rhodopsin conformations that exist in temperature- and pH-dependent photochemical equilibria (Schafer et al. 2016; Van Eps et al. 2017), where corresponding kinetic rates are strongly associated in vivo with the recovery rate of dark adaptation (Frederiksen et al. 2016), as well as overall rod photosensitivity (Imai et al. 2007; Yue et al. 2017). In particular, the spontaneous thermal decay rate of the inactive dark-state conformation and the decay rate of the light-activated MII conformation are two distinct nonspectral functional properties considered evolutionary innovations to dim light (Aho et al. 1988; Imai et al. 1997; Lamb et al. 2016; Yue et al. 2017). It is precisely the conformational stability of the rhodopsin dark and active states, which directly governs the photochemistry and kinetic rates of these physiologically important rod equilibria described above (Schafer et al. 2016; Van Eps et al. 2017). It is therefore highly likely that the conformational stability of rhodopsin indirectly modulates these properties of rod photoreceptors strongly associated with animal visual performance (Aho et al. 1988; Kefalov et al. 2003; Imai et al. 2007; Frederiksen et al. 2016; Yue et al. 2017). As ectotherms restricted to cold high altitude environments (Schaefer et al. 2011; Ma et al. 2016), Andean and Himalayan catfish specialists are likely to experience slowed biochemical processes relative to closely related taxa at lowland temperatures (Siddiqui and Cavicchioli 2006; Fields et al. 2015; Åqvist 2017). Mutations destabilizing the rhodopsin conformation would therefore be an elegant and parsimonious tuning mechanism by which natural selection could accelerate and therefore functionally compensate for thermally slowed rod activation kinetics at high altitudes (Castiglione et al. 2017).

Natural high-altitude variants from both Andean and Himalayan catfish RH1 may have therefore been specifically targeted by selection to accelerate RH1 kinetic rates at high altitudes. In contrast, other mutations at conserved positions within the visual opsins can increase protein stability and consequently decelerate the kinetic rates of dark- and active-state rhodopsin decay (Imai et al. 1997; Stojanovic et al. 2003; Xie et al. 2003; Dungan and Chang 2017; Morrow et al. 2017; Yue et al. 2017). Moreover, rhodopsin mutations affecting these kinetic rates often also produce pleiotropic effects altering the spectral absorbance (λ_{MAX}) of rhodopsin (Gozem et al. 2012; Luk et al. 2016; Yue et al. 2017). In comparison, we found that high altitude specific Andean and Himalayan catfish RH1 mutations had purely nonspectral functional effects. This nonspectral functional adaptation is in contrast to many cases where rhodopsin spectral sensitivity is targeted by selection and shifted in response to spectral conditions (Hunt et al. 2001; Yokoyama et al. 2008; Dungan et al. 2016). Our results here and previously (Castiglione et al. 2017) suggest sites 59 and 74 were targeted in response to temperature, specifically due to their functional effects on rhodopsin kinetics.

Although the spectral composition of ambient light changes with increasing altitude (Körner 2007), this is mostly due to an increase in the UV (Horvath 1993), which falls outside the spectral sensitivity of rhodopsin. Furthermore, changes in atmospheric gases (i.e., ozone) appear to have minor effects on overall light attenuation between high and low altitudes (Horvath 1993). This suggests that the changes in rhodopsin kinetics we describe here are not likely due to convergent spectral differences at high altitudes relative to lowland environments, especially since we investigated catfishes from clear mountainous drainages (Sommaruga et al. 1999; Castiglione et al. 2017). By contrast, small decreases in temperature such as those between high and low altitude environments (Castiglione et al. 2017) directly affect rhodopsin-mediated visual performance in ectotherms (Aho et al. 1988). The expected effects of spectrally consistent visual ecologies, but shifting environmental temperatures are supported by our structural and functional characterizations of rhodopsin: both the Andean (L59Q) and Himalayan (Y74F) mutations are located outside of the RBP controlling rhodopsin spectral tuning (Hunt et al. 2001; Yokoyama et al. 2008). By contrast, both substitutions are located near several members of a highly conserved intramolecular GPCR hydrogen bond network controlling rhodopsin kinetics (Ernst et al. 2014). Variation in the membrane-facing Andean (59) and Himalayan (74) sites under selection are near different hubs of this important rhodopsin domain, and when mutated in vitro (L59Q, Y74F), both variants accelerated these physiologically important decay rates that are associated with the pigment's nonspectral temperature-sensitive functions.

Parallel shifts in evolutionary rates at Andean and Himalayan catfish RH1 sites may therefore improve visual performance in cold high-altitude environments where these important kinetic rates of rhodopsin are likely slowed relative to warm lowland environments (Siddiqui and Cavicchioli 2006; Castiglione et al. 2017). The process of functional adaptation in a protein can be detected as a change in the evolutionary rates of the encoding gene (Elde et al. 2009; Patel et al. 2012), with selection pressures such as positive selection capable of driving adaptive amino acid substitutions in response to environmental variables (Castiglione et al. 2017; Dungan and Chang 2017; Hauser et al. 2017). In contrast to a widespread relaxation of selective constraint, such as in the rhodopsin of blind cavefishes (Niemiller et al. 2013), the acceleration of selective constraint we detect here is largely driven by sites 59, 74, and 288 where we previously detected robust evidence of positive selection on sites 59 and 288 within the Andean high-altitude specialist (Castiglione et al. 2017). Our functional and structural results are consistent with protein functional phenotypes observed in cold-adapted

enzymes, where unlike thermophilic enzymes (Nguyen et al. 2016), a well-established activity and stability trade-off has been repeatedly demonstrated in cold-adapted enzyme proteins from taxa as diverse as bacteria, archaea, and vertebrates (Siddiqui and Cavicchioli 2006; Fields et al. 2015; Åqvist 2017). Our structural and functional analyses bear striking similarities to the molecular mechanisms underlying this stability-activity trade-off, where accelerated kinetic rates are often achieved through single amino acid substitutions in membrane-facing regions where conformational shifts occur (Fields et al. 2015). The molecular mechanisms of protein cold adaptation, combined with the strong similarities in structural context and functional effects shared by RH1 sites 59 and 74, likely explains why these membrane-facing sites were targeted by parallel selection pressures within Andean and Himalayan catfishes physiologically restricted to high altitudes and cold temperatures (Peng et al. 2004; Schaefer and Arroyave 2010; Schaefer et al. 2011).

MOLECULAR CONVERGENCE IN RHODOPSIN REFLECTS SIMILAR MACROEVOLUTIONARY TRANSITIONS

Our results also reaffirm the presence of similar environmental pressures between Andean (*Astroblepus*) and Himalayan (Glyptosternoids) high-altitude catfish habitats, evidenced by the convergent macroevolutionary high-altitude specializations of these two groups. In contrast to the altitude generalists from each region, which display much less pronounced morphological adaptations to high altitude torrent zones (Guo et al. 2005; Peng et al. 2006; Schaefer et al. 2011), *Astroblepus* and the glyptosterninae contain different, but functionally convergent morphological adaptations that prevent dislodgement in these extreme hydrologic environments (Lujan and Conway 2015). Furthermore, *Astroblepus* and glyptosternoids are likely physiologically confined to high altitude Andean and Himalayan environments, respectively (Peng et al. 2004; Schaefer and Arroyave 2010), with recent evidence supporting adaptation to hypoxia in the glyptosternoids (Ma et al. 2016). Evidence of strong positive and divergent selection on the branch leading to glyptosternoid *rh1* provided in this study is similar to the positive and divergent selection we detected on the *rh1* of *Astroblepus* rhodopsin (Castiglione et al. 2017), where in both analyses these unique molecular evolutionary patterns were absent from the *rh1* of the altitude generalists from both geographic regions (Guo et al. 2005; Peng et al. 2006; Schaefer et al. 2011). Although perhaps unintuitive, our molecular evolutionary analyses of a visual protein therefore support the macroevolutionary specializations of both Andean and Himalayan high-altitude groups, raising questions about what other genes and phenotypes may be functionally convergent between these two groups. Our work on rhodopsin builds on previous studies finding evidence of convergent selection pressures at the molecular level between species that display convergent morphological adaptions to shared ecological variables (Chikina et al. 2016; Rubin and Moreau 2016; Partha et al. 2017).

PARALLEL SHIFTS IN EVOLUTIONARY RATES CAN IDENTIFY FUNCTIONAL CONVERGENCE IN PROTEINS

Our results also have implications for protein evolution, where molecular convergence in function underlain by nonparallel amino acid substitutions is an exciting new field of study (Manceau et al. 2010; Natarajan et al. 2016). Although epistasis, pleiotropy, and historical contingency may constrain protein functional convergence to be mediated by a limited number of parallel amino acid substitutions (Stern 2013; McGlothlin et al. 2016; Storz 2016), nonparallelism can exist across a wide-range of proteins: GPCRs as demonstrated here in rhodopsin and previously in the melanocortin-1 receptor (Mc1r) receptor (Manceau et al. 2010; Rosenblum et al. 2010), sodium channels (Feldman et al. 2012), metabolic antifreeze proteins (Chen et al. 1997), as well as hemoglobin (Jessen et al. 1991; Natarajan et al. 2016). The overall prevalence of amino acid parallelism versus nonparallelism in protein functional convergence may depend on the tendency of a given protein function to be mediated by global versus local structural mechanisms. This is evidenced by the strong amino acid parallelism underlying molecular convergence in rhodopsin spectral tuning (Hunt et al. 2001; Yokoyama et al. 2008), where electrostatic interactions within the RBP restrict the proximity of spectral tuning sites to a certain set of positions capable of altering the electronic configuration of the chromophore (Kochendoerfer et al. 1999). By contrast, the kinetic properties of visual pigments and other class A GPCRs can be potentially modulated via multiple junctions of the hydrogen bond network that spans nearly the entire protein structure (Ernst et al. 2014), where mutations on the periphery can directly or indirectly mediate kinetic rates involved in activation and stability (Castiglione et al. 2017; Dungan and Chang 2017). In instances of nonparallel amino acid substitutions, predicting adaptive functional convergence from coding-sequence data alone may therefore require a preexisting understanding of the structural mechanisms mediating the protein function in question.

This places a restrictive burden on predictive investigations of adaptive molecular convergence using genomic datasets, where detailed structural and functional information may be lacking. This is exacerbated by a methodological reliance on amino acid parallelism, which may preclude the discovery of nonparallel instances of functional convergence (Chen et al. 1997; Protas et al. 2006; Natarajan et al. 2016). Our approach employed codon-based models of molecular evolution to identify parallel shifts in d_N/d_S between organisms displaying convergent phenotypes—a detection method that does not necessarily rely on the presence of amino acid parallelism nor preexisting structural

knowledge (although such information is valuable for putting evolutionary rates into perspective; Castiglione et al. 2017). Our study tested for parallel shifts in site-specific d_N/d_S using models designed to detect clade-specific patterns in codon substitution rates. The strength of these models is the ability to statistically evaluate multiple evolutionary hypotheses (Schott et al. 2014; Castiglione et al. 2017; Hauser et al. 2017) using nested null models (Bielawski and Yang 2004; Schott et al. 2014) via likelihood-ratio tests (Anisimova and Liberles 2007; Weadick and Chang 2012) and Bayesian approaches to site-identification (Yang et al. 2005). This statistical approach allows expectations of divergence in evolutionary rates (ω_d) between two or more clades to be statistically evaluated against other hypotheses, such as parallelism. The advantage of d_N/d_S approaches for identifying candidate sites mediating protein functional convergence is the lack of a priori assumptions of which sites may be involved. Although parallel shifts in d_N/d_S can only describe similar shifts in evolutionary rates—not similar shifts in protein function—neither shifts in evolutionary rates (Chikina et al. 2016; Rubin and Moreau 2016; Partha et al. 2017), nor similarities in amino acid substitutions (Foote et al. 2015; Storz 2016; Dungan and Chang 2017) are guarantees of adaptive functional convergence in proteins (Cheviron et al. 2014; Thomas and Hahn 2015; Zou and Zhang 2015b). This makes experimental validation an essential component for computational predictions of protein adaptation (Rosenblum et al. 2010; Foote et al. 2015; Natarajan et al. 2016), which are especially important for predictions of molecular convergence because intramolecular epistasis can constrain parallel amino acid substitutions to drive divergent aspects of protein function (Storz 2016; Dungan and Chang 2017).

For high-altitude rhodopsin coding sequences, parallelism in evolutionary rates identified functional convergence in rhodopsin proteins, an understanding which may be especially useful in elucidating other nonparallel instances of molecular convergence. The magnitude of the functional shifts induced by the Andean and Himalayan mutations differs substantially, even though these two sites are evolving under a parallel shift in selective constraint and are located only 8 Å apart, each proximal to the same rhodopsin functional motifs. This highlights a previously underexplored relationship between evolutionary rate and functional convergence, which we hypothesize to be governed by a complex relationship that may depend on the structural mechanisms governing a protein's evolution. For example, variation in structural constraints may explain the diversity of nonparallel mechanisms underlying adaptive convergence in some experimental evolution studies (e.g. Tenaillon et al. 2012). How these structural and functional dynamics interact with environmental constraints to shape evolutionary rates and molecular convergence in proteins should be more widely investigated.

AUTHORS CONTRIBUTION

GMC and BSWC conceived the study and wrote the paper with assistance from FEH and RKS. GMC collected and analyzed all data with assistance from RKS, FEH, and BSWC.

ACKNOWLEDGMENTS

This work was supported by a National Sciences and Engineering Research Council (NSERC) Discovery grant (BSWC) and Vision Science Research Program Scholarships (GMC, RKS, FEH). The 11-*cis*-retinal was generously provided by Rosalie Crouch (Medical University of South Carolina). We also thank N. K. Lujan (University of Toronto Scarborough) for helpful discussions. The authors declare that there are no financial competing interests associated with this research.

DATA ARCHIVING

Rhodopsin (Rh1) sequences analyzed in this study were obtained from Genbank. Accession numbers are listed in tables S1–S4.

LITERATURE CITED

Aho, A., K. Donner, C. Hyden, L. Larsen, and T. Reuter. 1988. Low retinal noise in animals with low body temperature allows high visual sensitivity. Nature 334:348–350.

Aminetzach, Y. T., J. R. Srouji, C. Y. Kong, and H. E. Hoekstra. 2009. Convergent evolution of novel protein function in shrew and lizard venom. Curr. Biol. 19:1925–1931.

Anisimova, M., and D. A. Liberles. 2007. The quest for natural selection in the age of comparative genomics. Heredity 99:567–579.

Anisimova, M., J. P. Bielawski, and Z. Yang. 2001. Accuracy and power of the likelihood ratio test in detecting adaptive molecular evolution. Mol. Biol. Evol. 18:1585–1592.

Åqvist, J. 2017. Cold adaptation of triosephosphate isomerase. Biochemistry 56:4169–4176.

Beall, C. M. 2007. Two routes to functional adaptation: Tibetan and Andean high-altitude natives. Proc. Natl. Acad. Sci. USA 104:8655–8660.

Bielawski, J. P., and Z. Yang. 2004. A maximum likelihood method for detecting functional divergence at individual codon sites, with application to gene family evolution. J. Mol. Evol. 59:121–32.

Bofkin, L., and N. Goldman. 2007. Variation in evolutionary processes at different codon positions. Mol. Biol. Evol. 24:513–521.

Brodie, E. D. 2010. Convergent evolution: pick your poison carefully. Curr. Biol. 20:152–154.

Castiglione, G. M., F. E. Hauser, B. S. Liao, N. K. Lujan, A. Van Nynatten, J. M. Morrow, R. K. Schott, N. Bhattacharyya, S. Z. Dungan, and B. S. W. Chang. 2017. Evolution of nonspectral rhodopsin function at high altitudes. Proc. Natl. Acad. Sci. 114:7385–7390.

Chen, L., A. L. DeVries, and C. H. Cheng. 1997. Convergent evolution of antifreeze glycoproteins in Antarctic notothenioid fish and Arctic cod. Proc. Natl. Acad. Sci. USA 94:3817–3822.

Chen, W.-J. J., S. Lavoué, and R. L. Mayden. 2013. Evolutionary origin and early biogeography of otophysan fishes (Ostariophysi: Teleostei). Evolution. 67:2218–2239.

Cheviron, Z. A., C. Natarajan, J. Projecto-Garcia, D. K. Eddy, J. Jones, M. D. Carling, C. C. Witt, H. Moriyama, R. E. Weber, A. Fago, et al. 2014. Integrating evolutionary and functional tests of adaptive hypotheses: a case study of altitudinal differentiation in hemoglobin function in an Andean sparrow, *Zonotrichia capensis*. Mol. Biol. Evol. 31:2948–2962.

Chikina, M., J. D. Robinson, and N. L. Clark. 2016. Hundreds of genes experienced convergent shifts in selective pressure in marine mammals. Mol. Biol. Evol. 33:2182–2192.

Cortesi, F., Z. Musilová, S. M. Stieb, N. S. Hart, U. E. Siebeck, M. Malmstrøm, O. K. Tørresen, S. Jentoft, K. L. Cheney, N. J. Marshall, et al. 2015. Ancestral duplications and highly dynamic opsin gene evolution in percomorph fishes. Proc. Natl. Acad. Sci. USA 112:1493–1498.

Dungan, S. Z., and B. S. W. Chang. 2017. Epistatic interactions influence terrestrial–marine functional shifts in cetacean rhodopsin. Proc. R. Soc. B Biol. Sci. 284. https://doi.org/10.1098/rspb.2016.2743.

Dungan, S. Z., A. Kosyakov, and B. S. Chang. 2016. Spectral tuning of killer whale (*Orcinus orca*) rhodopsin: evidence for positive selection and functional adaptation in a cetacean visual pigment. Mol. Biol. Evol. 33:323–336.

Ebrey, T., and Y. Koutalos. 2001. Vertebrate photoreceptors. Prog. Retin. Eye Res. 20:49–94.

Elde, N., S. Child, A. Geballe, and H. Mlik. 2009. Protein kinase R reveals an evolutionary model for defeating viral mimicry. Nature 457:485–489.

Endler, J. 1986. Natural selection in the wild. Princeton Univ. Press, Princeton, NJ.

Ernst, O. P., D. T. Lodowski, M. Elstner, P. Hegemann, L. S. Brown, and H. Kandori. 2014. Microbial and animal rhodopsins: structures, functions, and molecular mechanisms. Chem. Rev. 114:126–163.

Feldman, C. R., E. D. Brodie, and M. E. Pfrender. 2012. Constraint shapes convergence in tetrodotoxin-resistant sodium channels of snakes. Proc. Natl. Acad. Sci. 109:4556–4561.

Fields, P. A., Y. Dong, X. Meng, and G. N. Somero. 2015. Adaptations of protein structure and function to temperature: there is more than one way to "skin a cat." J. Exp. Biol. 218:1801–1811.

Foote, A. D., Y. Liu, G. W. C. Thomas, T. Vinař, J. Alföldi, J. Deng, S. Dugan, C. E. van Elk, M. E. Hunter, V. Joshi, et al. 2015. Convergent evolution of the genomes of marine mammals. Nat. Genet. 47:272–275.

Frederiksen, R., S. Nymark, A. V Kolesnikov, J. D. Berry, L. Adler, Y. Koutalos, V. J. Kefalov, and M. C. Cornwall. 2016. Rhodopsin kinase and arrestin binding control the decay of photoactivated rhodopsin and dark adaptation of mouse rods. J. Gen. Physiol. 148:1–11.

Govardovskii, V. I., N. Fyhrquist, T. O. M. Reuter, D. G. Kuzmin, and K. Donner. 2000. In search of the visual pigment template. Vis. Neurosci. 17:509–528.

Gozem, S., I. Schapiro, N. Ferre, and M. Olivucci. 2012. The molecular mechanism of thermal noise in rod photoreceptors. Science. 337:1225–1228.

Gregory-Wodzicki, K. M. 2000. Uplift history of the central and northern Andes: a review. GSA Bull. 112:1091–1105.

Guo, X., S. He, and Y. Zhang. 2005. Phylogeny and biogeography of Chinese sisorid catfishes re-examined using mitochondrial cytochrome b and 16S rRNA gene sequences. Mol. Phylogenet. Evol. 35:344–362.

Guo, Y., S. Sekharan, J. Liu, V. S. Batista, J. C. Tully, and E. C. Y. Yan. 2014. Unusual kinetics of thermal decay of dim-light photoreceptors in vertebrate vision. Proc. Natl. Acad. Sci. USA 111:10438–10443.

Hauser, F. E., K. L. Ilves, R. K. Schott, G. M. Castiglione, H. López-Fernández, and B. S. W. Chang. 2017. Accelerated evolution and functional divergence of the dim light visual pigment accompanies cichlid colonization of Central America. Mol. Biol. Evol. 34:2650–2664.

Hayes, J. P., C. S. O. Connor, J. P. Hayes, and C. S. O. Connor. 1999. Natural selection on thermogenic capacity of high-altitude deer mice. Evolution 53:1280–1287.

Hedges, S., M. Suleski, M. Paymer, and S. Kumar. 2015. Tree of life reveals clock-like speciation and diversification. Mol. Biol. Evol. 32:835–845.

Hofmann, K. P., P. Scheerer, P. W. Hildebrand, H. W. Choe, J. H. Park, M. Heck, and O. P. Ernst. 2009. A G protein-coupled receptor at work: the rhodopsin model. Trends Biochem. Sci. 34:540–552.

Horvath, H. 1993. Atmospheric light absorption—a review. Atmos. Environ. A Gen. Top. 27:293–317.

Hughes, C., and R. Eastwood. 2006. Island radiation on a continental scale: exceptional rates of plant diversification after uplift of the Andes. Proc. Natl. Acad. Sci. USA 103:10334–10339.

Hunt, D. M., K. S. Dulai, J. C. Partridge, P. Cottrill, and J. K. Bowmaker. 2001. The molecular basis for spectral tuning of rod visual pigments in deep-sea fish. J. Exp. Biol. 204:3333–3344.

Imai, H., D. Kojima, T. Oura, S. Tachibanaki, A. Terakita, Y. Shichida, N. Academy, and U. States. 1997. Single amino acid residue as a functional determinant of rod and cone visual pigments. Proc. Natl. Acad. Sci. USA 94:2322–2326.

Imai, H., V. Kefalov, K. Sakurai, O. Chisaka, Y. Ueda, A. Onishi, T. Morizumi, Y. Fu, K. Ichikawa, K. Nakatani, et al. 2007. Molecular properties of rhodopsin and rod function. J. Biol. Chem. 282:6677–6684.

Jessen, T. H., R. E. Weber, G. Fermi, J. Tame, and G. Braunitzer. 1991. Adaptation of bird hemoglobins to high altitudes: demonstration of molecular mechanism by protein engineering. Proc. Natl. Acad. Sci. USA 88:6519–6522.

Kefalov, V., Y. Fu, N. Marsh-Armstrong, and K.-W. Yau. 2003. Role of visual pigment properties in rod and cone phototransduction. Nature 425:526–531.

Kochendoerfer, G. G., S. W. Lin, T. P. Sakmar, and R. a Mathies. 1999. How color pigments are tuned. Trends Biochem. Sci. 24:300–305.

Körner, C. 2007. The use of "altitude" in ecological research. Trends Ecol. Evol. 22:569–574.

Lamb, T. D., H. Patel, A. Chuah, R. C. Natoli, W. I. L. Davies, N. S. Hart, S. P. Collin, and D. M. Hunt. 2016. Evolution of vertebrate phototransduction: cascade activation. Mol. Biol. Evol. 33:2064–2087.

Losos, J. B. 2011. Convergence, adaptation, and constraint. Evolution. 65:1827–1840.

Löytynoja, A., and N. Goldman. 2008. Phylogeny-aware gap placement prevents errors in sequence alignment and evolutionary analysis. Science 320:1632–1635.

Lujan, N. K., and K. W. Conway. 2015. Life in the fast lane: a review of rheophily in freshwater fishes. Pp. 107–136 *in* R. Riesch, M. Tobler, and M. Plath, eds. Extremophile fishes: ecology, evolution, and physiology of teleosts in extreme environments. Springer, Cham, Switzerland.

Luk, H. L., N. Bhattacharyya, F. Montisci, J. M. Morrow, F. Melaccio, A. Wada, M. Sheves, F. Fanelli, B. S. W. Chang, and M. Olivucci. 2016. Modulation of thermal noise and spectral sensitivity in Lake Baikal cottoid fish rhodopsins. Sci. Rep. 6. https://doi.org/10.1038/srep38425.

Ma, X., W. Dai, J. Kang, L. Yang, and S. He. 2016. Comprehensive transcriptome analysis of six catfish species from an altitude gradient reveals adaptive evolution in Tibetan fishes. G3 6:1–33.

Manceau, M., V. S. Domingues, C. R. Linnen, E. B. Rosenblum, and H. E. Hoekstra. 2010. Convergence in pigmentation at multiple levels: mutations, genes and function. Philos. Trans. R. Soc. B Biol. Sci. 365:2439–2450.

McGlothlin, J. W., M. E. Kobiela, C. R. Feldman, T. A. Castoe, S. L. Geffeney, C. T. Hanifin, G. Toledo, F. J. Vonk, M. K. Richardson, E. D. Brodie Jr., et al. 2016. Historical contingency in a multigene family facilitates adaptive evolution of toxin resistance. Curr. Biol. 26:1616–1621.

Morrow, J. M., G. M. Castiglione, S. Z. Dungan, P. L. Tang, N. Bhattacharyya, F. E. Hauser, and B. S. W. Chang. 2017. An experimental comparison of human and bovine rhodopsin provides insight into the molecular basis of retinal disease. FEBS Lett. 591:1720–1731.

Natarajan, C., F. G. Hoffmann, R. E. Weber, A. Fago, C. C. Witt, and J. F. Storz. 2016. Predictable convergence in hemoglobin function has unpredictable molecular underpinnings. Science 354:336–339.

Nevado, B., G. W. Atchison, C. E. Hughes, and D. A. Filatov. 2016. Widespread adaptive evolution during repeated evolutionary

radiations in New World lupins. Nat. Commun. 7. https://doi.org/10.1038/ncomms12384.

Nguyen, V., C. Wilson, M. Hoemberger, J. B. Stiller, R. V Agafonov, S. Kutter, J. English, D. L. Theobald, and D. Kern. 2016. Evolutionary drivers of thermoadaptation in enzyme catalysis. Science. 355:289–294.

Niemiller, M. L., B. M. Fitzpatrick, P. Shah, L. Schmitz, and T. J. Near. 2013. Evidence for repeated loss of selective constraint in rhodopsin of amblyopsid cavefishes (teleostei: Amblyopsidae). Evolution. 67:732–748.

Okada, T., M. Sugihara, A. N. Bondar, M. Elstner, P. Entel, and V. Buss. 2004. The retinal conformation and its environment in rhodopsin in light of a new 2.2 Å crystal structure. J. Mol. Biol. 342:571–583.

Palczewski, K. 2006. G protein-coupled receptor rhodopsin. Annu. Rev. Biochem. 75:743–767.

Parker, J., G. Tsagkogeorga, J. A. Cotton, Y. Liu, P. Provero, E. Stupka, and S. J. Rossiter. 2013. Genome-wide signatures of convergent evolution in echolocating mammals. Nature 502:1–9.

Partha, R., B. Chauhan, Z. Ferreira, J. Robinson, K. Lathrop, K. Nischal, N. Clark, and M. Chikina. 2017. Subterranean mammals show convergent regression in ocular genes and enhancers, along with adaptation to tunneling. eLife 6. https://doi.org/10.7554/eLife.25884.

Patel, M. R., Y.-M. Loo, S. M. Horner, M. Gale, and H. S. Malik. 2012. Convergent evolution of escape from hepaciviral antagonism in primates. PLoS Biol. 10:e1001282.

Peng, Z., S. He, and Y. Zhang. 2004. Phylogenetic relationships of glyptosternoid fishes (Siluriformes: Sisoridae) inferred from mitochondrial cytochrome b gene sequences. Mol. Phylogenet. Evol. 31:979–987.

Peng, Z., S. Y. W. Ho, Y. Zhang, and S. He. 2006. Uplift of the Tibetan plateau: evidence from divergence times of glyptosternoid catfishes. Mol. Phylogenet. Evol. 39:568–572.

Projecto-Garcia, J., C. Natarajan, H. Moriyama, R. E. Weber, A. Fago, Z. A. Cheviron, R. Dudley, J. A. McGuire, C. C. Witt, and J. F. Storz. 2013. Repeated elevational transitions in hemoglobin function during the evolution of Andean hummingbirds. Proc. Natl. Acad. Sci. USA 110:20669–20674.

Protas, M. E., C. Hersey, D. Kochanek, Y. Zhou, H. Wilkens, W. R. Jeffery, L. I. Zon, R. Borowsky, and C. J. Tabin. 2006. Genetic analysis of cavefish reveals molecular convergence in the evolution of albinism. Nat. Genet. 38:107–111.

Rosenblum, E. B., H. Römpler, T. Schöneberg, and H. E. Hoekstra. 2010. Molecular and functional basis of phenotypic convergence in white lizards at White Sands. Proc. Natl. Acad. Sci. USA 107:2113–2117.

Royden, L. H., B. C. Burchfiel, and R. D. van der Hilst. 2008. The geological evolution of the Tibetan plateau. Science 321:1054–1058.

Rubin, B. E. R., and C. S. Moreau. 2016. Comparative genomics reveals convergent rates of evolution in ant–plant mutualisms. Nat. Commun. 7. https://doi.org/10.1038/ncomms12679.

Schaefer, S. 2011. The Andes: riding the tectonic uplift. Pp. 259–278 *in* J. S. Albert and R. E. Reis, eds. Historical biogeography of neotropical freshwater fishes. Univ. of California Press, Berkeley, CA.

Schaefer, S. A., and J. Arroyave. 2010. Rivers as islands: determinants of the distribution of Andean astroblepid catfishes. J. Fish Biol. 77:2373–2390.

Schaefer, S. A., P. Chakrabarty, A. J. Geneva, and M. H. Sabaj Pérez. 2011. Nucleotide sequence data confirm diagnosis and local endemism of variable morphospecies of Andean astroblepid catfishes (Siluriformes: Astroblepidae). Zool. J. Linn. Soc. 162:90–102.

Schafer, C. T., J. F. Fay, J. M. Janz, and D. L. Farrens. 2016. Decay of an active GPCR: conformational dynamics govern agonist rebinding and persistence of an active, yet empty, receptor state. Proc. Natl. Acad. Sci. 113:11961–11966.

Schott, R. K., S. P. Refvik, F. E. Hauser, H. López-Fernández, B. S. W. Chang, H. Lopez-Fernandez, and B. S. W. Chang. 2014. Divergent positive selection in rhodopsin from lake and riverine cichlid fishes. Mol. Biol. Evol. 31:1149–1165.

Siddiqui, K. S., and R. Cavicchioli. 2006. Cold-adapted enzymes. Annu. Rev. Biochem. 75:403–433.

Sommaruga, R., R. Psenner, E. Schafferer, K. A. Koinig, and S. Sommaruga-Wograth. 1999. Dissolved organic carbon concentration and phytoplankton biomass in high-mountain lakes of the Austrian Alps: potential effect of climatic warming an UV underwater attenuation. Arct. Antarct. Alp. Res. 31:247–253.

Stern, D. L. 2013. The genetic causes of convergent evolution. Nat. Rev. Genet. 14:751–764.

Stojanovic, A., I. Hwang, H. G. Khorana, and J. Hwa. 2003. Retinitis pigmentosa rhodopsin mutations L125R and A164V perturb critical interhelical interactions: new insights through compensatory mutations and crystal structure analysis. J. Biol. Chem. 278:39020–39028.

Storz, J. F. 2016. Causes of molecular convergence and parallelism in protein evolution. Nat. Rev. Genet. 17:239–250.

Storz, J. F., S. J. Sabatino, F. G. Hoffmann, E. J. Gering, H. Moriyama, N. Ferrand, B. Monteiro, and M. W. Nachman. 2007. The molecular basis of high-altitude adaptation in deer mice. PLoS Genet. 3:e45.

Sugawara, T., H. Imai, M. Nikaido, Y. Imamoto, and N. Okada. 2010. Vertebrate rhodopsin adaptation to dim light via rapid meta-II intermediate formation. Mol. Biol. Evol. 27:506–519.

Sullivan, J. P., J. G. Lundberg, and M. Hardman. 2006. A phylogenetic analysis of the major groups of catfishes (Teleostei: Siluriformes) using rag1 and rag2 nuclear gene sequences. Mol. Phylogenet. Evol. 41:636–662.

Tenaillon, O., A. Rodriguez-Verdugo, R. L. Gaut, P. McDonald, A. F. Bennett, A. D. Long, and B. S. Gaut. 2012. The molecular diversity of adaptive convergence. Science 335:457–461.

Thomas, G. W. C., and M. W. Hahn. 2015. Determining the null model for detecting adaptive convergence from genomic data: a case study using echolocating mammals. Mol. Biol. Evol. 32:1232–1236.

Van Eps, N., L. N. Caro, T. Morizumi, A. K. Kusnetzow, M. Szczepek, K. P. Hofmann, T. H. Bayburt, S. G. Sligar, O. P. Ernst, and W. L. Hubbell. 2017. Conformational equilibria of light-activated rhodopsin in nanodiscs. Proc. Natl. Acad. Sci. 114:E3268–E3275.

Venkatakrishnan, A. J., X. Deupi, G. Lebon, F. M. Heydenreich, T. Flock, T. Miljus, S. Balaji, M. Bouvier, D. B. Veprintsev, C. G. Tate, et al. 2016. Diverse activation pathways in class A GPCRs converge near the G-protein-coupling region. Nature 536:484–487.

Verberk, W. C. E. P., D. T. Bilton, P. Calosi, and S. J. I. 2011. Oxygen supply in aquatic ectotherms: partial pressure and solubility together explain biodiversity and size patterns. Ecology 92:1565–1572.

Weadick, C. J., and B. S. W. Chang. 2012. An improved likelihood ratio test for detecting site-specific functional divergence among clades of protein-coding genes. Mol. Biol. Evol. 29:1297–300.

Xie, G., A. K. Gross, and D. D. Oprian. 2003. An opsin mutant with increased thermal stability. Biochemistry 42:1995–2001.

Xing, Y., and R. H. Ree. 2017. Uplift-driven diversification in the Hengduan Mountains, a temperate biodiversity hotspot. Proc. Natl. Acad. Sci. USA 114:E3444–E3451.

Yang, Z. 2007. PAML 4: phylogenetic analysis by maximum likelihood. Mol. Biol. Evol. 24:1586–1591.

Yang, Z., W. S. W. Wong, and R. Nielsen. 2005. Bayes empirical Bayes inference of amino acid sites under positive selection. Mol. Biol. Evol. 22:1107–1118.

Yokoyama, S., T. Tada, H. Zhang, and L. Britt. 2008. Elucidation of phenotypic adaptations: molecular analyses of dim-light vision proteins in vertebrates. Proc. Natl. Acad. Sci. USA 105:13480–13485.

Yue, W. W. S., R. Frederiksen, X. Ren, D.-G. Luo, T. Yamashita, Y. Shichida, M. C. Cornwall, and K.-W. Yau. 2017. Spontaneous activation of visual pigments in relation to openness/closeness of chromophore-binding pocket. Elife 6:1–13.

Zhou, C., X. Wang, X. Gan, Y. Zhang, D. M. Irwin, R. L. Mayden, and S. He. 2016. Diversification of Sisorid catfishes (Teleostei: Siluriformes) in relation to the orogeny of the Himalayan plateau. Sci. Bull. 61:991–1002.

Zou, Z., and J. Zhang. 2015a. Are convergent and parallel amino acid substitutions in protein evolution more prevalent than neutral expectations? Mol. Biol. Evol. 32:2085–2096.

———. 2015b. No genome-wide protein sequence convergence for echolocation. Mol. Biol. Evol. 32:1237–1241.

Associate Editor: D. Filatov
Handling Editor: M. Servedio

Supporting Information

Additional Supporting Information may be found in the online version of this article at the publisher's website:

Figure S1. Species tree of Sisoridae used in molecular evolutionary analyses of *rh1*.
Figure S2. Siluriform and characiform species relationships used in molecular evolutionary analyses of RH1.
Figure S3. Schematic of amino acid variation at sites 59 and 74 across the phylogenetic dataset (Fig. S2).
Table S1. List of sisorid species for which rhodopsin (rh1) was analyzed.
Table S2. List of characiform species for which rhodopsin (rh1) was analyzed.
Table S3. Genbank accession numbers for lowland tropical and subtropical RH1.
Table S4. Andean (*Astroblepus, Ancistrus*) *rh1* sequences from our previous study (Castiglione et al., 2017).
Table S5. Results of Clade Model C (CmC) analyses of high altitude *rh1* using distortions of the siluriform species tree.
Table S6. *rh1* sites inferred to be under accelerated evolutionary rates (CmC) within analyses of different partitioning schemes of the Andean and Himalayan phylogenetic dataset.
Table S7. Codon and encoded amino acids variants at sites 59 and 74 in Andean (*Astroblepus*) and Himalayan (glyptosterninae) high-altitude catfish specialists.
Table S8. Vertebrate species names and respective rhodopsin coding sequence accession numbers that were consulted for confirming that unique natural variants only occur within Andean and Himalayan rhodopsins at sites 59 and 74, respectively.